Impact of Mutations within the Putative Ca^{2+}-Binding Lumenal Interhelical a−b Loop of the Photosystem II D1 Protein on the Kinetics of Photoactivation and H_2O-Oxidation in *Synechocystis* sp. PCC6803†

Ming Qian,‡ Luan Dao,‡ Richard J. Debus,§ and Robert L. Burnap*,‡

Department of Microbiology and Molecular Genetics, Oklahoma State University, Stillwater, Oklahoma 74078, and Department of Biochemistry, University of California at Riverside, Riverside, California 92521

Received September 29, 1998; Revised Manuscript Received March 10, 1999

ABSTRACT: Mutations D1−D59N and D1−D61E in the putative Ca^{2+}-binding lumenal interhelical a−b loop of the photosystem II (PSII) D1 protein [Chu, H. A., Nguyen, A. P., and Debus (1995), *Biochemistry 34*, 5839−5858] were further characterized in terms of S-state cycling and photoactivation. Bare platinum electrode measurements of centrifugally deposited O_2-evolving membranes isolated from the a−b loop mutants demonstrated a retarded appearance of O_2 following single turnover flashes, although not to the extent of retardation seen in the Δpsb0 mutant, which lacks the extrinsic manganese-stabilizing protein (MSP). Double flash measurements indicate that retarded O_2 release in mutants coincides with a decrease in overall PSII turnover during the S_3-[S_4]-S_0 transition. S_2 and S_3 decay measurements in the isolated membranes indicate that D1−D59N and D1−D61E have faster decays of these higher S-states in contrast to slowed decays in the Δpsb0 mutant. Measurements of the flash interval dependence of photoactivation indicate that intermediates of photoactivation [light-dependent assembly of the $(Mn)_4$ complex] are highly destabilized in the a−b loop mutants compared to both ΔpsbO and the wild-type: flash intervals of greater than 2 s result in the nearly complete decay of unstable photointermediate(s) in the D1−D59N and D1−D61E samples, whereas a similar loss does not occur until intervals even greater than 10 s in the ΔpsbO and wild-type samples. These results are consistent with a role for the residues D1−D59 and D1−D61 in modulating the redox properties of the higher S-states and, also, possibly in the binding the calcium ion involved in photoactivation.

Photosynthetic H_2O oxidation is catalyzed by the multisubunit photosystem II (PSII) complex embedded in the photosynthetic membranes of plants, algae, and cyanobacteria. During H_2O-oxidation, four electrons are extracted from two molecules of H_2O releasing O_2 and protons (for reviews, see refs *1* and *2*). The H_2O-splitting enzyme passes through a series of intermediate oxidation states termed S-states (S_i, where $i = 0-4$), corresponding, at least in part, to the stepwise oxidation of a cluster of four Mn ions $(Mn)_4$[1] that forms the catalytic core of the H_2O-splitting enzyme. Oxygen derived from the decomposition of substrate H_2O is released during the transition from the S_3 to the S_0 state (the S_4 state being an unstable intermediate). In the dark, a population of PSII centers typically relaxes to an S-state distribution of 75% S_1 and 25% S_0. Under these conditions, O_2 release is delayed until the 3rd flash and thereafter oscillates with a period of four with eventual dephasing of the oscillation due to misses and double hits. Y_z, the redox active tyrosine 161 of the reaction center D1 protein, forms the reactive interface between charge separation events in the photochemical reaction center and redox changes in the H_2O-splitting enzyme. It is established that oxidation of Y_z by reaction center chlorophyll $P680^+$ results in the formation of the neutral radical $Y_z^\bullet$ with the release of a proton coinciding with the transfer of an electron to $P680^+$. Current models under scrutiny postulate that $Y_z^\bullet$ abstracts protons (*1, 3*) or hydrogen atoms (*2, 4*) directly from substrate H_2O coordinated to the $(Mn)_4$.

In addition to Mn, the PSII complex requires Ca^{2+} and Cl^- ions for the expression of H_2O-oxidation activity. Depletion of these essential ions causes an inhibition of S-state cycling by rendering $Y_z^\bullet$ incapable of oxidizing the water-splitting enzyme poised in the higher S-states. Although the Ca^{2+} requirement has been studied intensively, the number and affinity of Ca^{2+}-binding sites and the mechanism by which Ca^{2+} activates H_2O-oxidation remains obscure. In general, measured Ca^{2+} binding and activating

† This work was funded by the National Science Foundation (MCB 9728754 to R.L.B.) and by the National Institutes of Health (GM 43496 to R.J.D.).

* To whom correspondence should be addressed. Phone: 405-744-7445. Fax: 405-744-6790. E-mail: burnap@biochem.okstate.edu.

‡ Oklahoma State University.

§ University of California at Riverside.

[1] Abbreviations: Chl, chlorophyll; DCBQ, 2,6-dichloro-*p*-benzoquinone; DCMU, 3-(3,4-dichlorophenyl)-1,1-dimethylurea, inhibits electron transport between Q_A and Q_B; HA, hydroxylamine (NH_2OH); a−b loop, lumenally exposed interhelical loop situated between transmembrane helices a and b of the D1 reaction center protein; Hepes, 4-(2-hydroxyethyl)-1-piperazineethanesulfonic acid; $(Mn)_4$, tetranuclear Mn cluster functioning in H_2O-oxidation; MSP, manganese-stabilizing protein, extrinsic 33 kDa PSII protein; *psbA*, gene encoding the reaction center D1 protein *psbO*, gene encoding the manganese-stabilizing protein; Y_Z, redox active tyrosine of the D1 protein acting as secondary electron donor of the reaction center.

10.1021/bi982331i CCC: $18.00
Published on Web 04/21/1999

Scheme 1

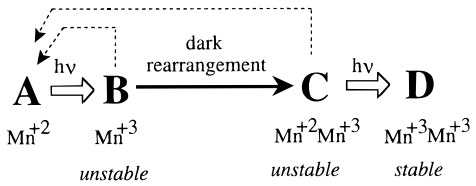

characteristics appear to depend strongly upon the experimental conditions, notably the Ca^{2+}-depletion procedures, the presence of competing cations, and complement of extrinsic polypeptides present. Furthermore, determination of the Ca^{2+}-binding constants is probably complicated by S-state dependent changes in the affinity and/or accessibility of the binding site. The identity of the ligands for PSII Ca^{2+} also remains unresolved. Mutational analysis has led to the tentative conclusion that D1−D59 and D1−D61 residues situated the interhelical lumenal loop of the D1 protein may be ligands of PSII Ca^{2+} (*5*). However, this conclusion is based upon in vivo assays of the autotrophic growth capacity of mutant cells grown with diminished concentrations of Ca^{2+} in the cell culture medium. It should be noted in this regard that increases in the Ca^{2+} requirement for autotrophic growth have also been reported for a number of other PSII mutations including replacement mutations in the C-terminal region of the D1 protein (*6, 7*) as well as for deletion mutants lacking the extrinsic proteins MSP (*8*) and cytochrome c_{550} (*9*).

As with the role of Ca^{2+} in the activation of H_2O-oxidation, the role of Ca^{2+} in the process of photoactivation remains unresolved. Photoactivation is the light-dependent ligation of Mn^{2+} into the H_2O-oxidation apo-complex of PSII culminating in the formation of an active enzyme containing Ca^{2+} and four $Mn^{\geq 3+}$. During photoactivation, the valency of Mn atoms increases from Mn^{2+} to $Mn^{\geq 3+}$ as the metal atoms become coordinated within the ligation environment of the active site. Photoactivation is a multiquantum process involving the existence of two unstable intermediates separated by a light-independent (dark) rearrangement step, typically with a 150 ms half-time (*10*−*12*). This kinetic model, termed the "two-quantum series model" (*10*), is shown in Scheme 1. The first quantum presumably corresponds to the photooxidation of Mn^{2+} and precedes a molecular rearrangement that is a prerequisite of the second photoevent, again a presumptive Mn^{2+} photooxidation. According to this model, the molecular rearrangement corresponds to the conversion of Mn^{3+} mononuclear intermediate (**B**) to the Mn^{3+}−Mn^{2+} binuclear complex (**C**). According to this model, the occurrence of the second photoevent effectively "locks in" the progress made through preceding steps. If, on the other hand, this "locking in" does not happen, the intermediates produced following the first photoevent are lost to decay processes.

There exists general consensus that Ca^{2+} and Mn^{2+} compete for each others' PSII-binding sites such that there is an optimal ratio for maximizing the yield of photoactivation (*11, 13*−*15*). Furthermore, it appears likely that low yields of photoactivation at low Ca^{2+} concentrations are due to destructive photoligation of Mn to inappropriate sites and that the binding of Ca^{2+} prevents this (*14, 16*). A crucial issue is whether Ca^{2+} is necessary for the photooxidative coordination of the Mn of the tetramer. The first experiments performed in vitro led to suggestions that Ca^{2+} was *not* necessary for the assembly of $(Mn)_4$ and could be added afterward to activate the otherwise assembled enzyme (*11, 14, 17, 18*). According to this model, the Ca^{2+} site is created upon the light-mediated formation of the $(Mn)_4$; that is, Ca^{2+} binding activates the nascent, and otherwise complete, $(Mn)_4$. Recent work using more rigorous Ca^{2+} depletion conditions, however, has led to the *opposite conclusion*, namely, that the binding of Ca^{2+} is a requisite intermediate step leading to the formation of the $(Mn)_4$ (*13, 16*). Using the tentative conclusion that D1−D59 and D1−D61 residues situated the interhelical lumenal loop of the D1 protein may be ligands of PSII Ca^{2+} (*5*), a structural model accounting for the dark rearrangement step of photoactivation has been proposed. According to this hypothesis, photoactivation is accompanied by a conformational change in the D1 protein, proposed to involve a rearrangement of the a−b loop and that this conformational rearrangement is coupled to the coordination of Ca^{2+} by the D1−D59 and D1−D61 residues (*12, 16*). Accordingly, the putative conformational rearrangement is hypothesized to correspond to the "dark rearrangement" stage of photoactivation that occurs between the absorption of the first and second light quanta during the sequential photooxidation and ligation of Mn atoms into the PSII H_2O-oxidation apo-protein. In the present study, we have analyzed the effects of mutations at the a−b loop putative Ca^{2+}-binding site residues D1−D59 and D1−D61. The mutations D1−D59N and D1−D61E had only moderate effects upon the H_2O-oxidation reactions, whereas the mutations did cause dramatic destabilization of one or both of the unstable intermediates in the two-quantum scheme of photoactivation. These results are discussed in the context of the model that D1−D59 and D1−D61 are indeed Ca^{2+} ligands and that Ca^{2+} is required for the formation of a photoactivation intermediate. We speculate that mutational perturbation of the Ca^{2+}-binding site renders the intermediate less stable than in the wild-type, but that once assembled, the properties of the mutant enzyme deviate less dramatically from the wild-type.

MATERIALS AND METHODS

Preparation of ΔpsbO, D1-D59N, and D1-D61E Samples. The naturally transformable, glucose-utilizing strain of *Synechocystis* sp. PCC6803 (*19*) was used in the construction of all of the strains described here. For routine manipulations, the wild-type and mutant cyanobacterial strains were grown on a rotary shaker in BG-11 media supplemented with 5 mM glucose at 32 °C. The construction of the strain designated ΔpsbO which lacks the entire *psbO* coding sequence has been described previously (*20*). Construction and characterization of the D1−D59N, D1−D61E strains have also been described previously (*5, 21*). Isolation of O_2-evolving membranes was performed as described previously (*22, 23*).

Oxygen Evolution Measurements. Cells in liquid culture were harvested by centrifugation at 4000*g* for 5 min at room temperature. Following harvest, cells were resuspended to a chlorophyll concentration of 200 μg mL^{-1} in HN buffer (10 mM Hepes and 30 mM NaCl pH 7.1) and maintained up to 2 h under illumination on a rotory shaker prior to experimental assay. Maximal rates of O_2-evolution were determined polarographically at 30° C using a Clark-type electrode at a final chlorophyll concentration of 10 μg mL^{-1}. Samples were resuspended in HN buffer supplemented with 1.0 mM DCBQ and 1 mM potassium ferricyanide, and oxygen evolution was

measured in response to heat-filtered, saturating red (>620 nm) illumination. Maximal rates of O_2-evolution of isolated thylakoids were measured in HMCS (50 mM Hepes, 5 mM $CaCl_2$, 10 $MgCl_2$, and 1 M sucrose, pH 7.2). In experiments testing the effects of varying concentrations of Ca^{2+} on oxygen evolution, solutions were Chelex-treated to remove residual Ca^{2+}, and acid-washed plasticware and glassware was utilized. Polarographic measurements using a centrifugal bare platinum electrode were conducted using an apparatus as described previously (*24*) and derived from published instrumental designs (*25, 26*). Flash illumination of centrifugally deposited thylakoid membranes was conducted without the Wratten No. 9 yellow filter that was used during the analysis of whole cell samples (*24, 27*). This was necessary since isolated thylakoids lack phycobilisomes (PSII light harvesting antennae), making it necessary to use higher light intensities to ensure actinic saturation of the entire population of centers in the cell-free sample. Xenon flash illumination (5 μs fwhm) was determined to be saturating by following O_2 signal amplitudes in control samples as a function of flash intensity using neutral density filters. Four microliters of membranes at a concentration of 800 μg Chl mL^{-1} was diluted into 400 μL of electrolyte measuring buffer consisting of HMCS (above) supplemented with 200 mM NaCl, and the membranes were centrifugally deposited at 18000*g* for 10 min onto the platinum surface of the electrode in Sorvall HB-4A swing-out rotor. Both membrane and whole cell samples were dark adapted for 10 min prior to the initiation of the flash sequence. In the absence of the Wratten yellow filter (membrane samples), the photoelectric flash artifact was more pronounced and was subtracted from the O_2 signals by using a DCMU-poisoned sample to obtain a set of photoelectric signals in the absence of O_2 evolution. The double-flash procedure of Bouges-Bocquet (*28*) was used to estimate the turnover time of PSII during the S_3-[S_4]-S_0 transition. Dark adapted samples were given a sequence of saturating xenon flashes (saturation determined using neutral density filters) with the time interval between the third and fourth flashes systematically varied between 100 and 50 000 μs using a computer controlled digital timer.

Photoactivation. Hydroxylamine (HA) extraction of PSII Mn was performed essentially according to ref *29* with modifications as described previously (*24, 30, 31*). Three milliliters of the resuspended cells were incubated with 2 mM HA added from a freshly prepared and neutralized 0.2 M HA stock solution. This and all subsequent steps prior to photoactivation were performed in complete darkness. After a 10 min incubation with gentle rotary shaking, the HA-treated cells were diluted with 10 mL of HN buffer and pelleted at 25 °C by 12000*g* for 6 min. The cells were resuspended in 10 mL of HNMC (10 mM HEPES, 30 mM NaCl, 1 mM $CaCl_2$, and 50 μM $MnCl_2$, pH 7.0) buffer with gentle agitation for about 10 min. This step was repeated three times, and on the last wash, the cells were resuspended in of HNMC buffer to 200 μg of Chl mL^{-1}. Inclusion of Mn and Ca in the wash buffers was found to improve the reproducibility of the results, as noted previously (*24*). All samples were kept on a shaker at 150 rpm at room temperature throughout the duration of the photoactivation experiment.

Photoactivation was conducted at room temperature with HA-extracted cells using a procedure similar to one that Gleiter et al. used to follow the photoactivation of dark-deactivated samples (*32*). Our initial assays of photoactivation used a Clark-type electrode to monitor the light-dependent reacquisition of O_2 evolution activity in hydroxylamine-extracted samples. More recently, we have employed a bare platinum electrode to monitor the reacquisition of O_2-evolving capacity under flashing light. This arrangement was found to provide similar kinetic results (cf. ref *24*). HA-treated cells in HN buffer were centrifuged to the surface of the electrode and O_2 yields were measured. Cells remained at the electrode surface throughout the course of the experiments as evidenced during control experiments showing virtually no changes in the amplitudes and shape of the amperometric signal. In contrast, samples that are intentionally disturbed (to promote partial resuspension of deposited cells) exhibit marked changes in the shape of the signal as well as lower signal amplitudes. Measurement of the development of O_2 evolution activity as a function of flash number was performed as follows. Samples on the electrode were given train of filtered yellow (Wratten no. 9) xenon lamp flashes at 4 Hz. This frequency was found to give near optimal yields for all samples used in the present experiments. Immediately after the train of photoactivating flashes, the electrode was polarized, and after 10 s, a train of measuring flashes was given at 4 Hz for 5 s with the O_2 yields being recorded. The amplitudes of the O_2 yields during the last four flashes of the measuring flash train were averaged and compared with the amplitudes of the last four O_2 yields under a similar train of measuring flashes in the same sample in its maximally photoactivated state (following approximately 1000 flashes for samples exhibiting high quantum yield of photoactivation or 4000 or more flashes for samples exhibiting low quantum yield).

RESULTS

O_2 Yield Patterns and Release Kinetics in Isolated Membranes. O_2-evolving thylakoid membranes were isolated from the wild-type and each of the mutants. Unlike membranes from the ΔpsbO, which lacks MSP, the activity of the a−b loop mutants, D1−D59N and D1−D61E, did not require the addition of >100 mM NaCl to the isolation buffer for the stabilization of O_2 evolution activity. Maximal rates of O_2 evolution of isolated membranes was generally >90% of corresponding rates of O_2 evolution in the whole cells used as starting material indicating minimal loss of activity during membrane isolation. The rates were consistent with previously determined values with ΔpsbO, D1−D59N, and D1−D61E exhibiting rates of 43, 28, and 48%, respectively, compared to the wild-type [100% = 520 μmol (mg of Chl)$^{-1}$ h^{-1}]. Experiments testing the effects of Ca^{2+} concentration in the range 60 μM to 20 mM on the maximal rates of O_2 evolution did not reveal any differences between the mutants and wild-type in the isolated membrane preparations: the mutants and the wild-type all showed modest and similar increase (approximately 20%) in activity going from 60 μM to 20 mM Ca^{2+}.

The O_2 evolution properties of membranes were investigated using a centrifugal bare platinum electrode. This electrode allows the deposition of the thylakoid membranes directly upon the platinum surface maximizing the kinetic sensitivity of measurements of O_2 release under single

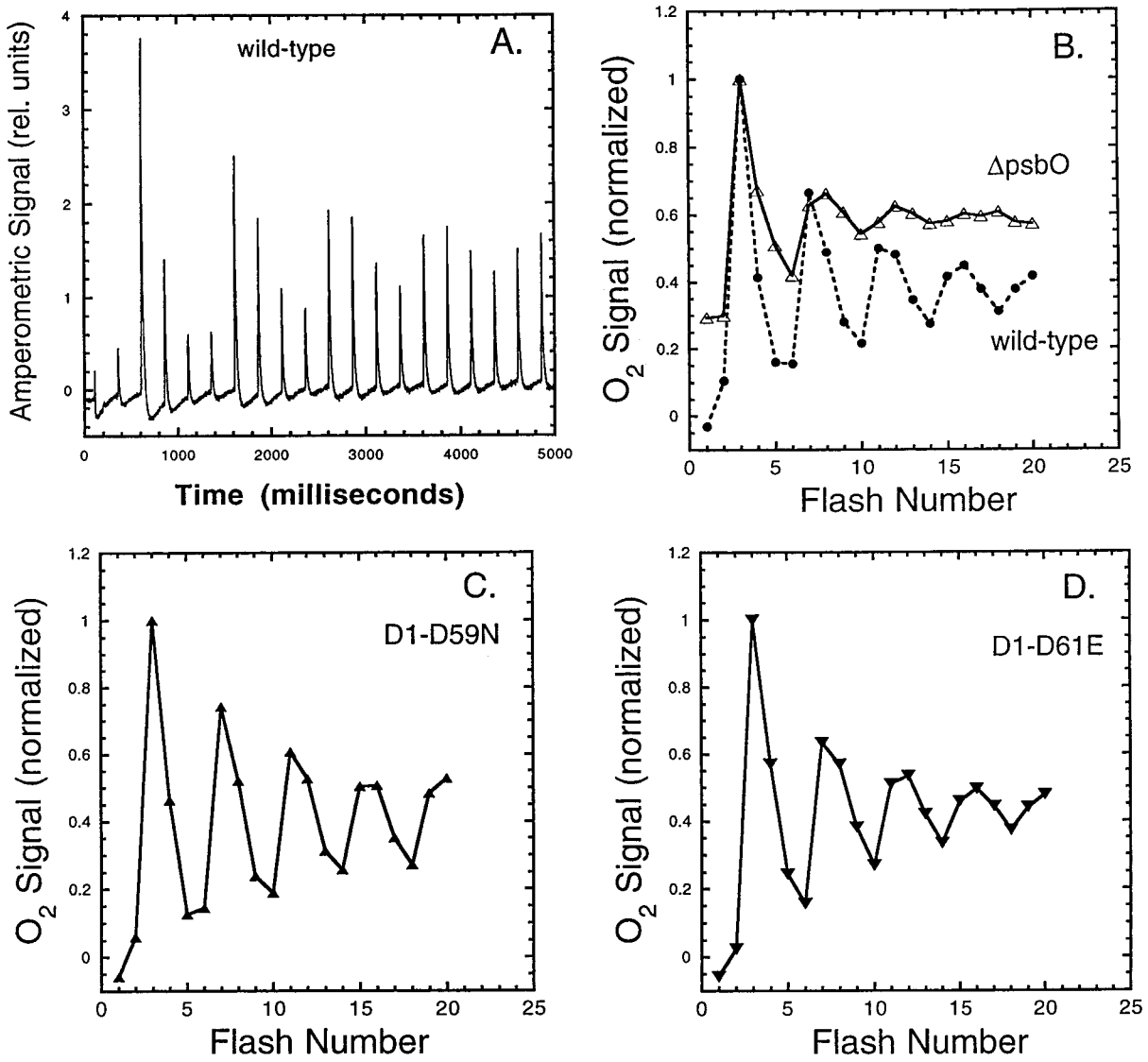

FIGURE 1: Flash O_2 yields of isolated membranes. Oxygen production by dark-adapted wild-type and mutant membranes that have been centrifugally deposited upon the surface of a bare-platinum electrode. Panel A shows a representative amperometric trace of O_2 yields obtained using the centrifugal membrane method with wild-type membranes. Panels B−D depict the oscillatory pattern of O_2 production as a function of flash number by wild-type, closed circles; ΔpsbO, open triangles; D1−D59N close triangles; and D1−D61E, closed inverted triangles. Membranes were centrifuged to the surface of a bare-platinum electrode, dark adapted for 10 min, and given a train of saturating xenon flashes at 4 Hz frequency.

turnover flash conditions. However, unlike whole cell samples previously analyzed using this technique, isolated membranes lack the terminal electron acceptors that provide a mechanism to reoxidize the electron transport chain and thus the pool of electron acceptors is potentially limiting. Figure 1A shows a representative amperometric trace of wild-type membranes deposited upon the electrode surface and subjected to a train of saturating flashes. The pattern of O_2 yield exhibits the expected period four oscillation with the individual signals exhibiting sharp rise and fall kinetics (see below). Some loss of signal amplitude is observed during the sequence of 20 flashes. These results suggest, therefore, that the pool of electron acceptors in the membrane-bound electron transport chain (or the rate at their reduced forms are auto-oxidized) becomes limiting, although the size of the pool is sufficient to prevent a drastic electron acceptor limitation even after 20 flashes. Note that the oscillation remains deep throughout the sequences.

Inspection of the patterns of O_2 yield indicate that all the mutants display characteristic period four oscillation in O_2 yield patterns with maximal yields occurring on the third flash (Figure 1, panels B−D). The wild-type and D1-a−b loop mutant membrane samples relax to an S-state distribution approaching the canonical 25% S_0 and 75% S_1 distribution after 10 min dark adaptation (Table 1). On the other hand, similarly dark-adapted ΔpsbO membranes do not reach this equilibrium during this dark period owing to the increased lifetime of the S_2 and S_3 state as quantified below. All samples, except for ΔpsbO membranes, exhibit very low miss factors (compared to in vivo parameters, not shown). This is likely a consequence of the relatively oxidized condition of the PQ pool in membrane samples. In whole cell samples, the redox pool is relatively reduced even after dark adaptation (*33*) and previous analysis (*34*) has demonstrated that photochemical misses increase as a function of an increasingly reduced condition of the PQ pool.

Table 1: S-state Cycling Parameters[a]

strain	10 min dark S-state distribution: $S_0/S_1/S_2/S_3$ (%)	misses (%), α	hits (%), β	double hits (%), γ
wild-type	24/74/2/0	9	88	3
ΔpsbO	14/66/7/13	18	78	4
D1−D59N	23/76/0//0	8	89	3
D1−D61E	26/74/0/0	10	86	4

[a] Samples were given a series of 20 preflashes prior to the 10 min dark period preceding the a series of measuring flashes. Numerical analysis of the amplitudes was performed using either 4- or 5-state models as described previously (*36, 50*). The 4- and 5-state models produced essentially equivalent results and no evidence for the presence of an S_{-1} "super-reduced" state in any of the samples could be demonstrated using the 5-step models.

To obtain information on the kinetics of O_2 release from the isolated membranes, the O_2 signals of the deposited membranes were examined. Preliminary experiments had indicated that electrode system (electrolyte + electrode + amplifier) had a response time of about 0.5−0.8 ms when NaCl was present at concentrations >150 mM. Thus, O_2 signals appearing with exponential rise kinetics in the time range of about 1.5 ms and greater were reasonably well resolved kinetically, provided that >150 mM NaCl was present in the sample. Indeed, as shown below, wild-type membrane samples produced signals with rise kinetics approaching 1−2 ms, which is the estimated rate of O_2 release in these samples. It was also observed that the amount of sample deposited on the electrode surface had a pronounced effect upon the kinetics of the electrode signal observed. This was expected because the rise kinetic of the O_2 signal is slowed as the diffusion path to the electrode surface increases [for theoretical treatment, see Lavorel (*35*)]. To give the fastest possible signal rise kinetics and still give a reasonable signal-to-noise ratio, it was necessary to optimize the thickness of the deposited layer of thylakoid membranes on the electrode surface. The optimal amount of deposited thylakoids giving the fastest transient was found to be approximately the same (∼500 ng of Chl/cm^2 electrode surface area), for all types (wild-type and mutants) of thylakoid membranes studied here. Following this optimization, the O_2 signal for wild-type membranes (Figure 2A and Table 2) exhibits a rapid rise reaching a maximum approximately 3−4 ms after the flash. A single-exponential fit to the initial slope provides an estimate of the exponential half rise time ($t_{1/2}$) of 1.3 ms. This value for the wild-type is in accord with previous estimates of O_2 release from intact PSII and demonstrates the high kinetic resolution of this electrode system (*36, 37*). By comparison, signals from centrifugally deposited whole cell wild-type samples reached a corresponding maximum approximately 10 ms after the flash with a corresponding $t_{1/2} \gg 4$ ms. Since the rise of the O_2 signal corresponds to the appearance of O_2 at the electrode surface, the results demonstrate that the H_2O-oxidation complex is situated significantly closer to the electrode surface in the membrane samples than in whole cell samples. It is also worth noting that the comparatively rapid rise kinetics were accompanied by rapid decay of the signal, which corresponds to diffusion of O_2 away from the electrode surface following the initial O_2 gush.

Analysis of the O_2 signal kinetics in mutant thylakoid samples showed that each of the mutants exhibit a retardation of kinetics of O_2 release (Figure 2B and Table 2). Consistent with previous results using whole cell samples, membranes from the ΔpsbO mutant were found to have dramatically slowed O_2 release (Figure 2B). With our better resolution, the half-time of this release is estimated to be $t_{1/2} = 6.7$ ms. The O_2 signal (Figure 2B and Table 2) from membranes from the D1−D59N mutant was only slightly slower than the wild-type, although the low O_2 activity and consequent low signal-to-noise ratio of these samples make a numerical estimate of the value unreliable. The O_2 signal from membranes from the D1−D61E mutant was found to be moderately slowed with $t_{1/2} = 3.5$ ms (Figure 2B and Table 2).

As with the assays of maximal O_2 evolution rates as a function of Ca^{2+} concentration, experiments testing the effects of [Ca^{2+}] on the magnitude and kinetics of O_2 did not disclose any differences between the mutants and wild-type in the range of 60 μM to 20 mM Ca^{2+}.

PSII Turnover. The PSII reactions can be estimated using double flash methods using the bare platinum electrode as previously developed (*28, 38*). PSII turnover during the O_2-yielding S_3-[S_4]-S_0 transition was examined by varying the time interval between the third and fourth flash (Δt, f3-f4) and monitoring the amount of the oxygen released after the seventh flash. At long intervals between flashes (>10 ms), the oxygen yield is maximal after the third and seventh flashes. However, when the interval between the third and fourth flash is very short, the O_2 yield after the seventh flash is low. This low yield is due to the fact that the fourth flash was not converted to S-state advancement. As the length of time between the third and fourth flashes is increased, the yield after the seventh flash increases because a larger fraction of the sample has recovered from the previous (third) flash. The amplitude of oxygen yield due to the seventh flash (normalized to the average yield of during the 20 flash sequence) as a function of Δt, f3-f4, the time interval between third and fourth flash, thus provides a measure of the turnover time during the S_3-[S_4]-S_0 transition. Using this technique, it was found that wild-type cells and wild-type membranes exhibit very similar turnover kinetics with the rate-limiting step during the S_3-[S_4]-S_0 transition being $t_{1/2} = 1.2$ and 1.6 ms, for cells and membrane samples, respectively. Similar analysis of ΔpsbO samples gave values of $t_{1/2} = 7.1$ and 8.3 ms for cells and membranes, respectively. Cells and membranes of the D1−D59N and D1−D61E mutants exhibited $t_{1/2}$ values intermediate to those of wild-type and ΔpsbO, consistent with the O_2 release kinetic estimates (Table 2 and Figure 2).

S-State Decay. Estimates of the decay of the higher S-states (i.e., S_2, S_3) can also be estimated using double flash methods using the bare platinum electrode (*25, 27, 39, 40*). To measure the decay of the S_2 state, membrane samples were given one flash followed by a variable time interval (Δt, f1-f2) followed by a sequence of flashes given at 250 ms intervals. As the interval Δt, f1-f2, becomes longer, the amount of O_2 release after the third flash (f3) of the sequence decreases due to the decay of the S_2 state ($S_2 \rightarrow S_1$). To measure the decay of the S_3 state, a pair of flashes was given 250 ms apart (Δt, f1-f2, = 250 ms), which advances the majority of PSII centers to the S_3-state. This is followed by a variable time interval (Δt, f2-f3) and the detection of O_2 release upon the third flash (f3). The amount of O_2 release upon f3 decreases as the variable interval Δt, f2-f3, becomes

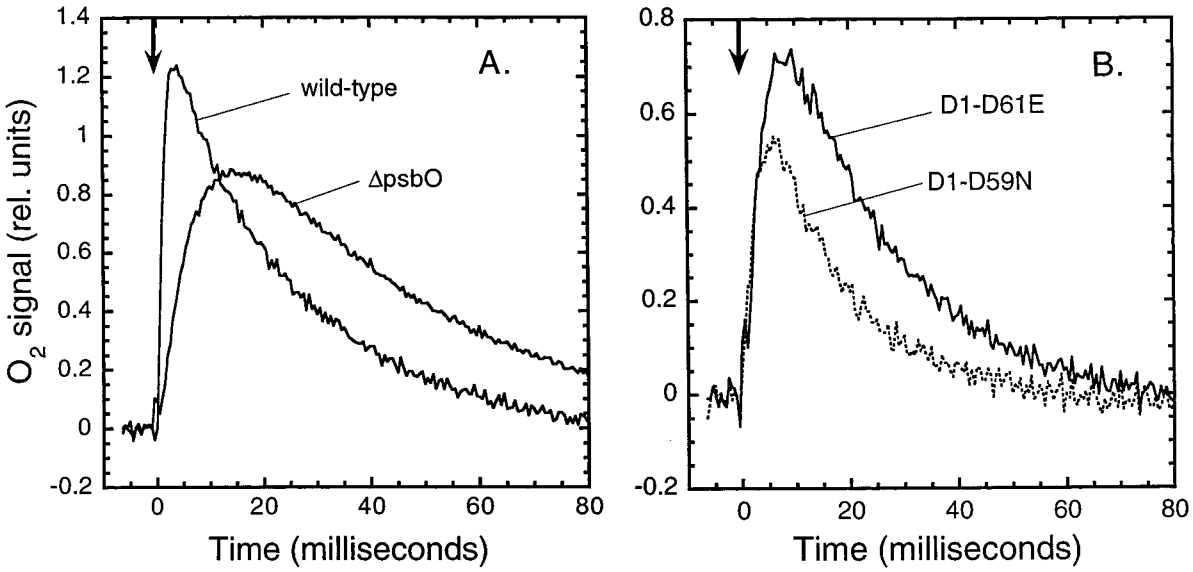

FIGURE 2: Oxygen signals of mutant and wild-type membranes. Oxygen signals of mutant and wild-type membranes centrifugally deposited upon the surface of a bare-platinum electrode and illuminated with saturating xenon flashes The exponential rise times of the depicted signals are given in Table 2. Kinetic analysis of the data was performed according to the exponential method described in Jursinic and Dennenberg (1990).

Table 2: Kinetics during the S_3-[S_4]-S_0 Transition

strain	O_2 release (ms),[a] $t_{1/2}$, membranes	PSII turnover (ms),[b] $t_{1/2}$, cells	PSII turnover (ms),[b] $t_{1/2}$, membranes	$Y_z^•$ reduction (ms),[c] $t_{1/2}$
wild-type	1.3	1.2	1.6	1.2[d]
ΔpsbO	6.7	7.1	8.3	6.0[e]
D1−D59N	1.9	1.9	1.8	nd
D1−D61E	3.5	5.5	3.8	nd

[a] Oxygen release kinetics were estimated from the rising portion of the O_2 signal (Figure 2) using the exponential method as described previously (*36, 37*). [b] Estimates of PSII turnover kinetics shown in Figure 3 was performed as described in and the Materials and Methods. Numerical analysis was performed by fitting to the equation of the form $Y_7/Y_{\text{steady state}} = 1 - e^{-kt}$ with $t_{1/2}$ obtained with the relation of $t_{1/2} = 0.693/k$. [c] Obtained from the literature. [d] Ref *47*. [e] Ref *55*.

longer and this decrease in yield is due to the decay of the S_3 state ($S_3 \rightarrow S_2$). Figure 4 shows the time course of the S_2 (top row) and S_3 (bottom row) lifetimes. The D1−D59N and D1−D61E mutants both exhibit faster decays of these higher S-states as compared to the wild-type. In contrast, the ΔpsbO mutant exhibits a slower decay. S-state decays could be fit with the model assuming two kinetic components as previously observed (Figure 4 and Tables 3 and 4). Fast components of decay are ascribed to the reduction of the S_2 or S_3 by reduced Y_D, whereas the slower components are due to reduction electron donation from the acceptor side (i.e., via Q_A) and perhaps other (ill-defined) endogenous donors (*40, 41*). Upon the basis of these considerations, we conclude that absence of MSP (ΔpsbO membranes) affects charge recombination with the acceptor side, but has little effect upon charge recombination with Y_D since the slow decay component is markedly retarded whereas the fast component is largely unaffected. On the other hand, the mutations in the D1-a−b loop appear to cause an acceleration of both pathways of charge recombination.

Photoactivation. To determine whether the site-directed mutations described here affect the kinetics of photoassembly of the $(Mn)_4$ cluster (photoactivation), cells were extracted with hydroxylamine (HA) to remove PSII active-site Mn and subjected to flash illumination to promote the light-dependent religation of active-site metals (*10, 24, 29, 31*). The experimental conditions employed maintain the availability of Mn^{2+}, Ca^{2+}, and Cl^- within the cells to ensure the presence of these necessary cofactors for the subsequent photoassembly of $(Mn)_4$ clusters. The flash number dependence of photoactivation provides a measure of the relative quantum yield of photoactivation as defined as the per flash increase the fraction of PSII centers capable of evolving O_2. Photoactivation is an inherently low quantum yield process [estimated at $<0.01-0.001$ depending upon the conditions (*13*)], and increases in the quantum yield are associated with increases in the probability of successful photoevents in which Mn-depleted PSII centers enter or continue the photoassembly sequence. Consistent with previous results (*24*), the genetic removal of MSP (ΔpsbO mutant strain) increases the relative quantum yield of photoactivation (Figure 5). As noted previously (*31*), this difference in kinetics is not due to changes in local concentrations of the Mn^{2+} or Ca^{2+} ions, since corresponding differences in relative quantum yield between the ΔpsbO and the wild-type are observed in samples that have been HA-extracted in the presence of EGTA and the divalent cation ionophore A23187: this treatment is photoactivation dependent upon addition of exogenous Mn^{2+} and Ca^{2+}, and photoactivation using optimal concentrations of these cations also occurs with an approximately 4-fold higher relative quantum yield in the ΔpsbO strain compared with the wild-type (Qian and Burnap, unpublished observations). As shown in Figure 5, the quantum yield of photoactivation the D1−D59N and D1−D61E mutants appears higher in comparison to the wild-type. However, closer inspection of the initial portions of the curve indicate that little difference between the a−b loop mutants or the wild-type is observed during the first 40−100 flashes and that the apparent differences in quantum yield only emerge later in the flash sequence for the a−b loop mutants. Since the level of reduction of the plastoquinone (PQ) pool is likely to affect the probability nonproductive back-reaction (i.e., charge recombination between PSII

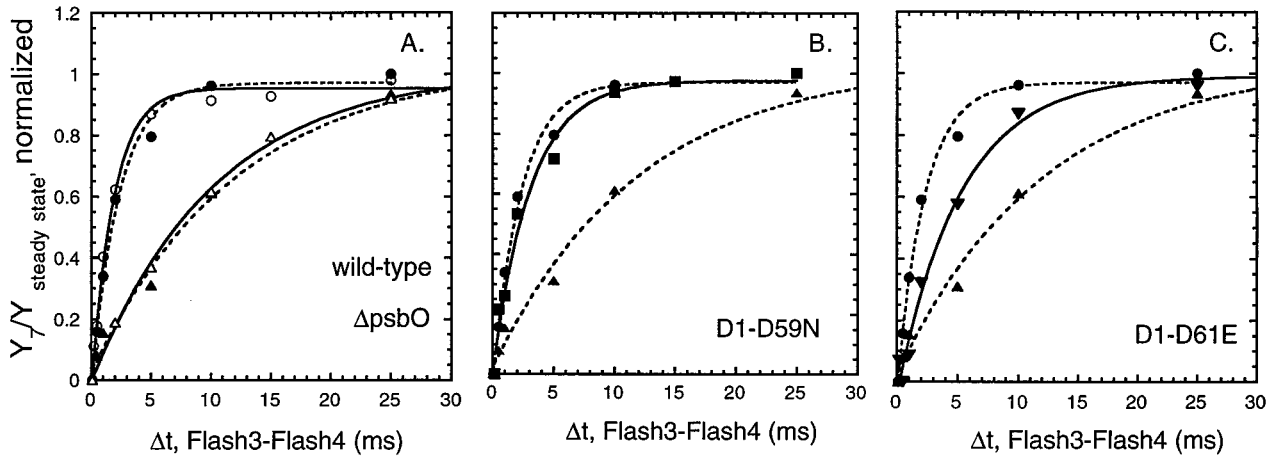

FIGURE 3: Double flash measurements of PSII enzyme turnover during the S_3-[S_4]-S_0 transition. (A) PSII turnover times during the O_2-yielding S_3-[S_4]-S_0 transition in wild-type cells (closed circles) and membranes (open circles) and ΔpsbO cells (open triangles) and membranes (closed triangles). (B) D1−D59N membranes (closed squares), wild-type membranes (closed circles, dotted line-fit), and ΔpsbO membranes (closed triangles, dotted line-fit). (C) D1−D61E membranes (closed inverted triangles), wild-type membranes (closed circles, dotted line-fit), and ΔpsbO membranes (closed triangles, dotted line-fit). Turnover times were estimated by varying the time interval between the third and fourth flash (Δ*t*, F3−F4) and detecting the amount of the oxygen released after the seventh flash (*28, 38*). The amplitude of oxygen yield due to the seventh flash (normalized to the average yield of during the 20 flash sequence) as a function of Δ*t*, F3−F4, the time interval between third and fourth flash, thus provides a measure of the turnover time during the S_3-[S_4]-S_0 transition. Lines represent fits according to the equation: $Y_7/Y_{steady\ state} = 1 - e^{-kt}$. Values of the fitted kinetic constants are shown in Table 2.

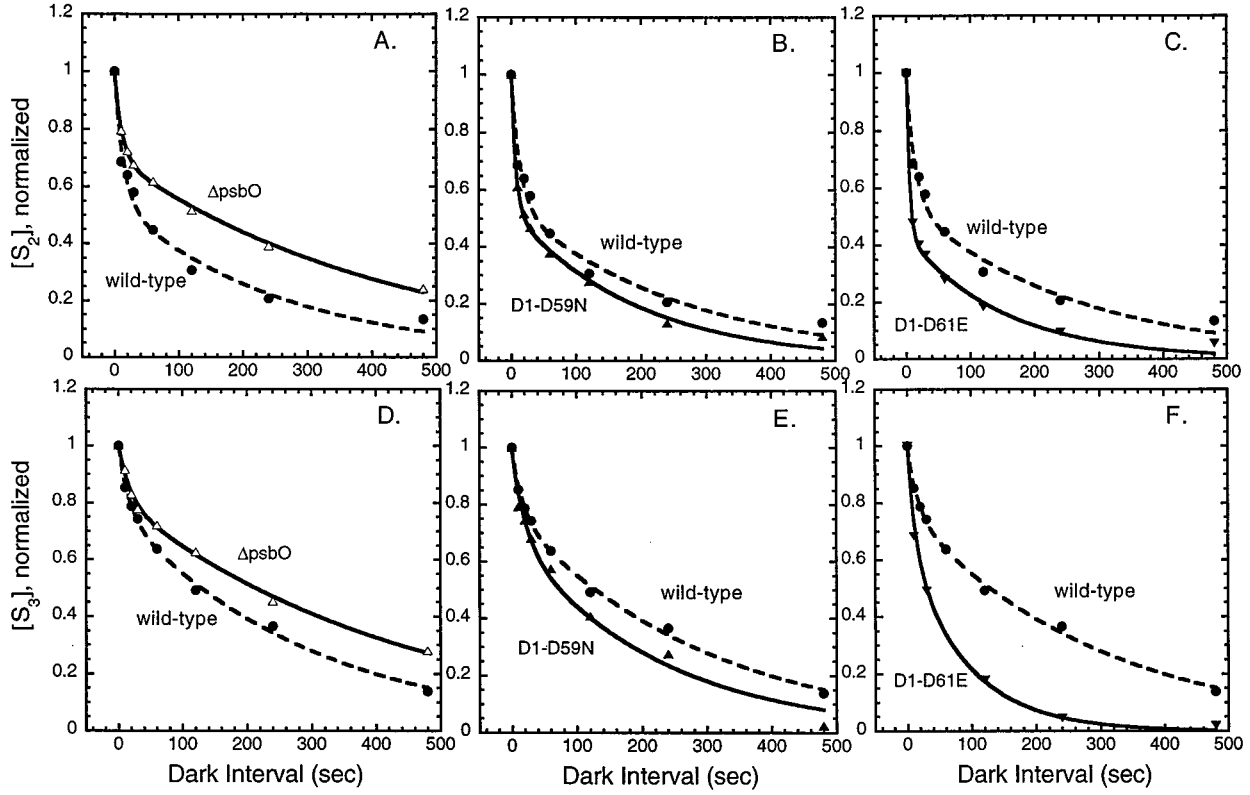

FIGURE 4: Decays of the S_2 and S_3 states. Decay of the S_2 state (panels A−C) and decay of the S_3 state (panels D−F) in membranes of the wild-type, closed circles; ΔpsbO, open triangles; D1−D59N closed triangles; and D1−D61E, closed inverted triangles. Measurements of the lifetimes of the S_2 state was performed by recording the amplitude of O_2 yield on the 3rd flash under conditions varying the time interval between the 1st and 2nd flashes. Measurement of the lifetime of the S_3 state in each of the different strains was performed by recording the amplitude of O_2 yield on the 3rd flash under conditions varying the time interval between the 2st and 3nd flashes (*25, 40, 56*).

electron acceptors and oxidant on the donor side), and since the mutants exhibit decreased concentrations of active PSII centers, it is reasonable to hypothesize that the observed differences in the quantum yield of photoactivation between the a−b loop mutants and the wild-type are due to higher levels of reduction of the PQ pool in the wild-type. It should be noted, however, that the photoactivation experiments were done in whole cells where the acceptor pool is much larger, in contrast to the isolated membranes where acceptor limitation is clearly a significant factor in the quantum yield of stable charge separation as shown above. Nevertheless, further experiments will be required to obtain a definitive answer for the basis of the differences in relative quantum yield of photoactivation between the wild-type and the a−b

Table 3: S_2 Decays[a]

strain	normalized extent, fast	$t_{1/2}$ (s), fast	normalized extent, slow	$t_{1/2}$ (s), slow
wild-type	44%	10	56%	180
ΔpsbO	30%	8	70%	297
D1−D59N	39%	3	61%	122
D1−D61E	57%	3	43%	106

[a] Data obtained as shown in Figure 4. Numerical analysis was performed by fitting to two exponentials described by kinetic constants k_i with $t_{1/2}$ obtained with the relation of $t_{1/2} = 0.693/k_i$.

Table 4: S_3 Decays[a]

strain	normalized extent, fast	$t_{1/2}$ (s), fast	normalized extent, slow	$t_{1/2}$ (s), slow
wild-type	22%	11	78%	204
ΔpsbO	19%	12	81%	304
D1−D59N	20%	5	80%	134
D1−D61E	28%	4	72%	59

[a] Data obtained as shown in Figure 4. Numerical analysis was performed by fitting to two exponentials described by kinetic constants k_i with $t_{1/2}$ obtained with the relation of $t_{1/2} = 0.693/k_i$.

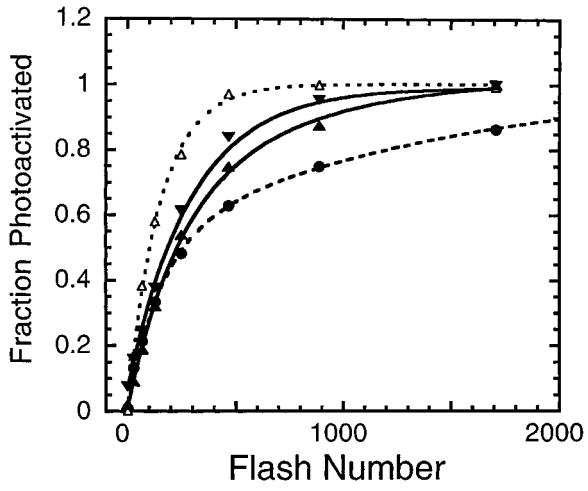

FIGURE 5: Photoactivation as a function of flash number in hydroxylamine-treated cells. Development of O_2 during a sequence of photoactivating flashes in Mn-extracted cells of the wild-type, closed circles; ΔpsbO, open triangles; D1−D59N closed triangles; and D1−D61E, closed inverted triangles. The photoactivating light consisted of a sequence of saturating, single turnover xenon flashes given at a fixed frequency of 4 Hz. Cells were centrifugally deposited on the electrode surface and subjected to the photoactivating flash sequence given without electrode polarization. Data points represent the normalized amplitudes of the O_2 signal obtained as the average O_2 signal amplitude of the last 4 flashes of a 20 flash 4 Hz measuring flash sequence on the polarized electrode initiated 10 s following the photoactivating flash sequence. Data points represent the averages of at least three experiments and the standard deviations at any point do not exceed 0.06 of maximal (1.0).

loop mutants, particularly as to why differences emerge later in the flash sequence.

The flash interval dependence of photoactivation was measured to assess possible kinetics of the rate-limiting steps and the lifetimes of unstable intermediate photoproducts of the multi-quantum photoactivation process (Scheme 1). Figure 6 shows the extent of photoactivation resulting from a fixed number of flashes given at different flash intervals in the wild-type, ΔpsbO, and D1 a−b loop mutant strains. All strains exhibit the characteristic bell shaped curve, presented in normalized form, observed both in vivo (*15, 24, 29*) and in vitro (*11, 13, 17, 18, 42*−*45*). To generate these curves, each of the strains was given a number of flashes that yield approximately 50% photoactivation, and therefore the curves all reach the same height despite rather different per flash quantum yields. The slope of the ascending portion of the curve is related to the rate constant of dark step(s) (*10, 18, 29*), whereas the overall slope and intercept of the descending portion of the curve depend on the lifetimes of the unstable intermediates. At very short spacing ($\Delta t <$ 50 ms), relatively lower yields of assembled centers are obtained reflecting the existence of a low quantum yield process initiating a dark step(s) that must go to completion before effective utilization of the next quantum occurs. The higher yields at these very short flash intervals are obtained in the D1−D61E mutant, ΔpsbO and, to a lesser extent in D1−D59N, are consistent with the higher relative quantum yields seen in Figure 6. The higher yields at the shortest flash intervals indicates that centers are more efficiently initiated or stabilized by some light-dependent step along the assembly pathway. The ascending slopes of the curve, which is related to the kinetic constant of the dark rearrangement (**B** → **C**, Scheme 1), are similar in all strains, and it therefore it appears that the intrinsic rate of the dark rearrangement step is not much altered by the mutations. Lower yields seen in all samples at long flash intervals (Figure 6), also reflects the multiquantum requirement of photoactivation, since it is expected that the product of the first quantum absorbed by the center has a greater probability of decaying if a second quantum arrives at a long time interval after the first. Interestingly, both the D1−D59N and D1−D61E mutants exhibit pronounced destabilization of intermediate(s) of $(Mn)_4$−Ca photoassembly, as evidenced by the more precipitous declines in the yields of photoactivation at the longer flash intervals, which is best observed when the data are presented in linear form with respect to the interval between flashes (Figure 6B). The optimum flash interval is comparatively much sharper in the a−b loop mutants. It is observed that, at dark intervals of greater than 2 s, most of the photointermediate(s) have decayed in the D1−D59N and D1−D61E samples, whereas a much smaller loss is observed in ΔpsbO and the wild-type samples at this flash interval.

DISCUSSION

Mutational studies have previously identified two highly conserved aspartate residues of the lumenal a−b loop of the D1 protein, D59 and D61, as possible ligands of Ca^{2+} associated with the PSII H_2O-oxidation complex (*5*). Such an assignment would be consistent with earlier predictions based upon sequence analysis (*46*). Here we have characterized the impact of mutations at these positions in terms of effects upon the S-state cycling properties of the PSII H_2O-oxidation reaction and the kinetics of the photoassembly of the $(Mn)_4$−Ca (=photoactivation). It was found that the D1−D61E mutant and, to a lesser extent, the D1−D59N mutant, exhibit alterations in the kinetics of the H_2O-oxidation reactions compared to the wild-type. Interestingly, both the D1−D59N and D1−D61E mutants were found to have quite pronounced alterations in the kinetics of photoactivation, notably a destabilization of an assembly intermediate hypothesized to require the presence of bound Ca^{2+}. On the

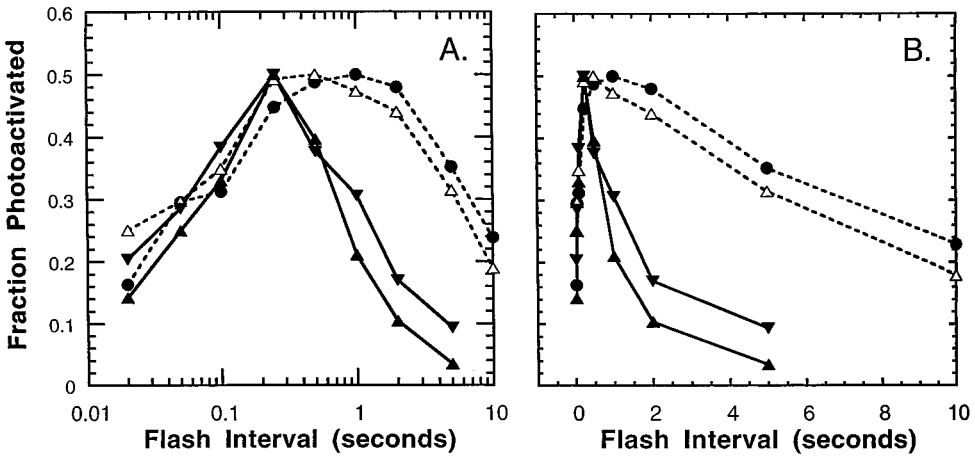

FIGURE 6: Photoactivation as a function of flash interval in hydroxylamine-treated cells. The flash interval dependence of photoactivation in Mn-extracted cells of the wild-type, closed circles; ΔpsbO, open triangles; D1−D59N closed triangles; and D1−D61E, closed inverted triangles. The data are presented in logarithmic and linear form with respect to the time interval. The samples were given fixed numbers of flashes given at different flash intervals ranging from 50 ms to 10 s. The number of flashes given to each sample was set to produce approximately 50% maximal photoactivation at 4 Hz for that particular sample. The data were further normalized to a value of 0.5 at the optimal flash frequency of the particular sample. After the fixed number of flashes was given at the indicated flash interval, the electrode polarization was turned on and a 4 Hz measuring flash sequence was applied as described in Figure 5. The electrode polarization was switched off and additional flashes were applied at 4 Hz to promote maximal photoactivation. The sample was then subjected to a 4 Hz measuring flash sequence with the electrode polarization switched on. The number of flashes required to obtain maximal photoactivation ranged from approximately 800 to 4000 flashes, according to the results in Figure 5. The data are presented as the amplitudes of the O_2 signal and have been normalized to 0.5 (reflecting the approximately 50% maximal photoactivation). Data points represent the averages of at least three experiments and the standard deviations at any point do not exceed 0.07 of maximal (0.5).

other hand, we were unable to observe any differences between the wild-type and the mutants with respect to the effect of added Ca^{2+} ions upon the H_2O-oxidation reaction in the fully assembled enzyme.

For the first time, membranes isolated from *Synechocystis* sp. PCC6803 mutants have been analyzed using a centrifugal bare platinum electrode (*25, 35*). This electrode permits the deposition of the membranes as a thin film on the electrode surface allowing a better time resolution of the kinetic transient of O_2 release from PSII following flash excitation when compared to a similar experiment using whole cell samples (*27, 30, 36*). Furthermore, the use of isolated membranes minimizes kinetic complications due to underlying slower transients that result from interactions between the photosynthetic and respiratory chains in whole cells (see below). Oxygen release occurs during the S_3-[S_4]-S_0 transition, which has a previously measured $t_{1/2}$ of approximately 1.2 ms as measured by the decay of $Y_z^{\bullet}$ reduction by the intact H_2O-oxidation complex. The 1.3 ms estimate of O_2 release obtained from the analysis of the O_2 signal from centrifugally deposited wild-type membranes is in good agreement with the previous estimates and is consistent with the idea that O_2 release kinetically coincides with the rate-limiting step during the S_3-[S_4]-S_0 transition. Previous analysis of whole cells had shown that the D1−D59N and D1−D61E mutations cause reductions in the maximal steady-state rates of DCBQ-supported O_2 evolution (to 33 and 61% compared to the wild-type rate, respectively). This previous analysis had also determined that the corresponding relative concentrations of charge-separating PSII were 65 and 80% relative to the wild-type, when taken together with the maximal rates of O_2 evolution, indicated that a fraction of the assembled PSII were nonfunctional and/or that enzyme turnover was slowed. The present experiments showed that O_2 release PSII is retarded during the S_3-[S_4]-S_0 transition in the a−b loop mutants, although the retardations are not as great as in the ΔpsbO strain (Figures 2 and 3, Table 2). It is also notable that O_2 release (as measured by appearance at the surface of the bare-platinum electrode, Figure 2) and the S_3-[S_4]-S_0 turnover kinetics of PSII (as obtained by double-flash measurements, Figure 3) were quite similar. This is consistent with the idea that the pace of events within the Y_z-H_2O-oxidation complex during the S_3-[S_4]-S_0 transition limit PSII turnover under flash illumination and that steps involved in the decomposition of substrate H_2O leading to O_2 release (H-abstraction from H_2O by $Y_z^{\bullet}$?) limit the progress of the S_3-[S_4]-S_0 transition (*47*). Recently, it was shown by Hundelt et al. that the D1−D61A and D1−D61N mutants have dramatically slowed O_2 release kinetics (*48*). In the same study, D1−D61E cells appeared to have normal O_2 release kinetics, at least at the resolution of the conditions employed (*48*). We attribute the different results regarding the D1−D61E mutants to reflect the fact that the techniques utilized in the present study on membrane samples allow more sensitive kinetic resolution of the O_2 signal than in the whole cell experiments employed by Hundelt et al.

The use of isolated membranes also eliminates possible interactions with metabolic reductant (*33*) that may affect the miss factor (*34*), the decay of higher S-states (present results), and interactions with the respiratory chain that are associated with intact cell samples (*49, 50*). Analysis of the oscillatory patterns of O_2 yield from isolated membranes demonstrate very low miss factors (α) (Figure 1 and Table 1) compared to similar measurements of intact cells (*27, 36*). This low miss factor is obtained despite the fact that PSII in these membrane samples has a much lower optical cross-section due to depletion of the phycobilisomes, which serve as the major PSII light harvesting antennae in cyanobacteria. The low miss factor is interpreted to reflect efficient reoxidation of PSII electron acceptors as a consequence of the relatively oxidized condition of the plastoquinone pool in accordance with previous analysis (*34*). In contrast, miss

factors are comparatively high in intact cyanobacterial cells presumably because of increases in backward transitions (dissipative charge recombinations) associated with a highly reduced PQ pool present in metabolically active *Synechocystis* cells (*33*).

Another consequence of the isolation of the membranes from potential metabolic interactions of the intact cell is the absence of a relatively slow ($t_{1/2} \approx 150$ ms) transients of positive deflection (apparent O_2 release), which are most clearly visible in whole cell samples undergoing respiration, but are absent in isolated membranes. These relatively slow transients are most readily seen following the first and second flashes in dark-adapted whole cell samples, but are convoluted into the usually much larger amplitude faster transients due to true O_2 production via H_2O-oxidation. The slow transients have been shown to be caused by the interaction between the photosynthetic and respiratory electron transport chains and represent an inhibition of respiratory O_2 uptake due to a competition for electrons between PSI and respiratory oxidase(s) (*49*). The slow respiratory transients are of fairly uniform magnitude in different PSII mutant strains in freshly harvested cells grown under similar conditions (unpublished observations), whereas the faster signals due to true O_2 production ($t_{1/2} \approx 5-16$ ms) obviously depend on the degree to which PSII is impaired by the mutations (*49*). Thus, in severely impaired mutants such as D1−D59N, the kinetics of photosynthetic O_2 release tend to be distorted in whole cells due to the convolution of the two types of signal and the fact that the faster photosynthetic O_2 signal is relatively smaller and the respiratory transient is, to a first approximation, unchanged.

A further difference between the isolated membrane and whole cells samples relates to the apparent the susceptibility of the $(Mn)_4$−Ca to endogenous reductants when samples are incubated in the dark. The formation of super-reduced forms of the H_2O-oxidation complex (S_{-1}- and S_{-2}-states) were not observed in the isolated membrane samples, whereas super-reduced forms of the H_2O-oxidation complex are routinely observed in dark-adapted cell samples (*24*, *50*, *51*). This disparity between membrane and whole cell samples is consistent with the interpretation that metabolically derived electrons, available in whole cells but absent in isolated membranes of all strains examined in this study, are capable of transfer to the $(Mn)_4$ in the dark and suggest that the formation of S_{-1}- and S_{-2}-states in vivo depends on the availability of metabolic reductants situated in the cytoplasm.

Differences between the isolated membrane and whole cells samples with respect to the availability of endogenous reductants also probably account for the fact that the S_2 and S_3 states are considerably more dark-stable (approximately 2-fold more long-lived) in the isolated membrane preparations measured here (Figure 4) in comparison to whole cell samples (cf. refs *25* and *27*). The more rapid S-state decays in the a−b loop mutants could be interpreted to indicate that the midpoint potential gap between Y_D and the higher S-states is increased. This situation might arise if the mutation caused the S_2/S_1 and S_3/S_2 midpoint potentials of $(Mn)_4$ complex to become more positive. This interpretation is consistent with the results of fluorescence experiments measuring charge recombination between Q_A^- and PSII electron donors in the D1−D59N and D1−D61E mutants (*5*).

Analysis of the S-state decay kinetics showed that the decays are well fit by assuming two kinetic components (Figure 4 and Tables 3 and 4), consistent with previous analyses using higher plant material (*39*, *40*). Previous analysis of the S_2 and S_3 decay indicated that the two kinetic components correspond to at least two pathways higher S-state deactivation. The fast component of the S_2 or S_3 decays are attributed to recombination between Y_D and the S_2- or S_3-state of the H_2O-oxidation complex. The slower component of the S_2 or S_3 decays are due to reduction of the H_2O-oxidation complex by an electron from the acceptor side of PSII or by other endogenous reductants (*39*, *40*). The faster decays in observed in both components of the S-state decays in the D1−D59N and D1−D61E mutants are again consistent with slightly more positive S_2/S_1 and S_3/S_2 midpoint potentials of $(Mn)_4$ complex which are similarly affecting both $Y_D \rightarrow (Mn)_4$ and acceptor side $\rightarrow (Mn)_4$ S-state deactivation pathways. On the other hand, the S_2 or S_3 decays in the ΔpsbO mutant appear considerably slower compared to the wild-type. However, analysis of the ΔpsbO decays reveals that the faster component, again presumably $Y_D \rightarrow (Mn)_4$, is comparable to the wild-type, whereas the slower component, assumed to correspond to charge recombination with the acceptor side is indeed considerably slower than the wild-type. The slower deactivation via the acceptor side $\rightarrow (Mn)_4$ pathway in ΔpsbO is in accord with previous fluorescence and thermoluminescence data (*36*, *52*). This suggests a decrease the midpoint potential gap between the PSII acceptor side and the higher S-states, which is in contrast to the supposed increase in the midpoint potential gap in the a−b loop mutants. At the same time, similar S-state deactivation via $Y_D \rightarrow (Mn)_4$ recombination suggests that the midpoint potential gap between Y_D and the higher S-states is probably similar to the wild-type. How does one explain a significantly smaller redox gap between the acceptor side and $(Mn)_4$, but a similar redox gap between Y_D and $(Mn)_4$? One possibility is that the absence of MSP causes the midpoint potential of Q_A^- to become more positive, but has little affect upon the midpoint potential of $(Mn)_4$. Such a proposal awaits experimental testing, yet existence of a transmembrane allosteric affect is not unprecedented: a shift in the midpoint of Q_A toward more positive potentials has been observed in higher plant PSII upon release of Ca^{2+} from the lumenal portion of PSII (*53*) and during photoactivation (*54*) similar to what is proposed here.

Perhaps the most intriguing aspect of the D1 a−b loop mutants concerns their photoactivation characteristics, particularly with respect to changes in the kinetics of the unstable intermediates along the assembly pathway. The D1−D59N and D1−D61E mutants each exhibited a dramatic decrease in the stability of the already unstable photoassembly intermediates **B** and/or **C** (two-quantum series model, Scheme 1) as evidenced by sharp drop-off in yields at long intervals between flashes (Figure 6). What factors could contribute to the observed destabilization of the photoactivation intermediates? At least three alternative explanations for the destabilization of the intermediates of photoactivation exist. First, the mutations may alter the redox properties of the photoactivation intermediates such that their decay via charge recombination more effectively competes with ad-

vancement through the assembly sequence. For example, photooxidized manganese in the partially assembled complex may become rereduced more rapidly by an electron from the acceptor side in a manner analogous to the hastened charge recombination between the higher S-states and the acceptor side in the fully assembled complex as shown above. Second, the mutation may produce structural alterations leading to enhanced accessibility to exogenous reductant thereby promoting reductive deactivation of the intermediates. Third, the mutations may impair binding of calcium and/or manganese ions following the first Mn^{2+} photooxidation presumed to occur during the **A** → **B** step of the two-quantum model.

Upon the basis of their most recent biochemical work, Cheniae's group argues that Ca^{2+} is required for the formation of $(Mn)_4$, and they speculate Ca^{2+} promotes the rearrangement (**B** → **C**) leading to the formation of the binuclear intermediate, although from their data it is not possible to ascertain which of the kinetic steps (formation of **B** or **C**) actually requires Ca^{2+}. More direct evidence that Ca^{2+} is involved in the intermediate stages in the formation of the $(Mn)_4$ has been obtained by the Dismukes' group who show that Ca^{2+} must bind before the second photooxidation can occur (*12*, *45*). Thus, their results specifically support the conjecture of Cheniae and co-workers that the binding of Ca^{2+} to D1−D59 and D1−D61 residues of the D1 a−b loop promotes a conformational change that corresponds to the dark rearrangement leading to the Mn^{3+}−Mn^{2+} binuclear complex (*12*, *16*). Assuming residues D1−D59 and D1−D61 coordinate Ca^{2+}, as suggested during the initial characterization of mutations at these positions (*5*), then the present results suggest that occupancy of this coordination site by Ca^{2+} is important for the formation or stabilization of one or both of the unstable photoassembly intermediates. We observed that varying the concentration of Ca^{2+} (60 μM to 20 mM) in assay buffers did not produce any differences between the putative Ca^{2+} binding a−b loop mutants and wild-type with respect to the O_2 evolution characteristics of isolated membranes. We speculate that the D1−D59 and D1−D61 residues indeed coordinate Ca^{2+}, but the dissociation constant for the putative D1−D59 and D1−D61 binding site and/or exchange rates for the Ca^{2+} at this site are too low to be detected under the conditions employed. On the other hand, no special efforts were made in this study to deplete the membranes of Ca^{2+} (e.g., NaCl/EDTA treatment), and efforts in this direction would be required to definitively address this issue. Nevertheless, the results of present experiments are consistent with the following hypothesis: the D1−D59N and D1−D61E mutations alter a Ca^{2+}-binding site whose occupancy is crucial for the photoassembly of the $(Mn)_4$. Once formed the PSII−$(Mn)_4$−Ca^{2+} complex functions in H_2O-oxidation, although the kinetic properties of the fully assembled $(Mn)_4$ are modified due to structural perturbations resulting from the Ca^{2+}-ligand mutations. However, until direct biochemical tests of the hypothesis that D1−D59 and D1−D61 coordinate Ca^{2+} are performed, the changes in the kinetics of photoactivation may be ascribed an alternative hypothesis; namely, that the mutations cause alterations in the redox properties of photoactivation intermediates rendering them more prone to decay.

REFERENCES

1. Britt, R. D. (1996) in *Oxygenic Photosynthesis: The Light Reactions* (Ort, D., and Yocum, C. F., Eds.) pp 137−164, Kluwer Academic Publishers, Dordrect, The Netherlands.
2. Diner, B. A., and Babcock, G. T. (1996) in *Oxygenic Photosynthesis: The Light Reactions* (Ort, D., and Yocum, C. F., Eds.) pp 213−247, Kluwer Academic Publishers, Dordrect, The Netherlands.
3. Gilchrist, M. L., Ball, J. A., Randall, D. W., and Britt, R. D. (1995) *Proc. Natl. Acad. Sci. U.S.A. 92*, 9545−9549.
4. Hoganson, C., Lydakis-Simantiris, N., Tang, X., Tommos, C., Warnke, K., Babcock, G., Diner, B., McCraken, J., and Styring, S. (1995) *Photosynth. Res. 46*, 177−184.
5. Chu, H. A., Nguyen, A. P., and Debus, R. J. (1995) *Biochemistry 34*, 5839−5858.
6. Nixon, P. J., and Diner, B. A. (1994) *Biochem. Soc. Trans. 22*, 338−43.
7. Chu, H. A., Nguyen, A. P., and Debus, R. J. (1995) *Biochemistry 3496*, 5859−5882.
8. Philbrick, J. B., Diner, B. A., and Zilinskas, B. A. (1991) *J. Biol. Chem. 266*, 13370−13376.
9. Shen, J. R., Qian, M., Inoue, Y., and Burnap, R. L. (1998) *Biochemistry 37*, 1551−1558.
10. Cheniae, G. M., and Martin, I. F. (1971) *Biochim. Biophys. Acta 253*, 167−181.
11. Tamura, N., and Cheniae, G. (1987) *Biochim. Biophys. Acta 890*, 179−194.
12. Zaltsman, L., Ananyev, G. M., Bruntrager, E., and Dismukes, G. C. (1997) *Biochemistry 36*, 8914−8922.
13. Ananyev, G. M., and Dismukes, G. C. (1996) *Biochemistry 35*, 4102−4109.
14. Miller, A.-F., and Brudvig, G. W. (1989) *Biochemistry 28*, 8181−8190.
15. Ono, T. A., and Inoue, Y. (1983) *Biochim. Biophys. Acta 723*, 191−201.
16. Chen, C., Kazimir, J., and Cheniae, G. M. (1995) *Biochemistry 34*, 13511−13526.
17. Tamura, N., Inoue, Y., and Cheniae, G. (1989) *Biochim. Biophys. Acta 976*, 173−181.
18. Miyao, M., and Inoue, Y. (1991) *Biochim. Biophys. Acta 1056*, 47−56.
19. Williams, J. G. K. (1988) *Methods Enzymol. 167*, 766−778.
20. Burnap, R., and Sherman, L. A. (1991) *Biochemistry 30*, 440−446.
21. Chu, H.-A., Nguyen, A. P., and Debus, R. A. (1994) *Biochemistry 33*, 6137−6149.
22. Burnap, R., Koike, H., Sotiropoulou, G., and Sherman, L. A. I. Y. (1989) *Photosynth. Res. 22*, 123−130.
23. Burnap, R. L., Qian, M., Shen, J. R., Inoue, Y., and Sherman, L. A. (1994) *Biochemistry 3307*, 13712−13718.
24. Burnap, R. L., Qian, M., and Pierce, C. (1996) *Biochemistry 35*, 874−882.
25. Nixon, P. J., and Diner, B. A. (1992) *Biochemistry 31*, 942−948.
26. Meunier, P. C., and Popovic, R. (1988) *Rev. Sci. Instrum. 59*, 486−491.
27. Putnam-Evans, C., Burnap, R., Wu, J., Whitmarsh, J., and Bricker, T. M. (1996) *Biochemistry 35*, 4046−4053.
28. Bouges-Bocquet, B. (1973) *Biochim. Biophys. Acta 292*, 772−785.
29. Cheniae, G. M., and Martin, I. F. (1972) *Plant Physiol. 50*, 87−94.
30. Burnap, R. L., Qian, M., Al-Khaldi, S., and Pierce, C. (1995) in *Photosynthesis: from light to biosphere* (Mathis, P., Ed.) Kluwer Academic Publishers, Dordrect, The Netherlands.
31. Qian, M., Al Khaldi, S. F., Putnam Evans, C., Bricker, T. M., and Burnap, R. L. (1997) *Biochemistry 36*, 15244−15252.
32. Gleiter, H. M., Haag, E., Shen, J. R., Eaton Rye, J. J., Seeliger, A. G., Inoue, Y., Vermaas, W. F., and Renger, G. (1995) *Biochemistry 34*, 6847−6856.
33. Mi, H., Endo, T., Ogawa, T., and Asada, K. (1995) *Plant Cell Physiol. 36*, 661−668.
34. Meunier, P. C. (1993) *Photosynth. Res. 36*, 111−118.
35. Lavorel, J. (1992) *Biochim. Biophys. Acta 1101*, 33−40.

36. Burnap, R., Shen, J. R., Jursinic, P. A., Inoue, Y., and Sherman, L. A. (1992) *Biochemistry 31*, 7404−7410.
37. Jursinic, P. A., and Dennenberg, R. J. (1990) *Biochim Biophys Acta 1020*, 195−206.
38. Diner, B. (1973) *Biochim. Biophys. Acta 305*, 353−363.
39. Messinger, J., and Renger, G. (1993) *Biochemistry 32*, 9379−9386.
40. Seeliger, A. G., Kurreck, J., and Renger, G. (1997) *Biochemistry 36*, 2459−2464.
41. Vass, I., and Styring, S. (1991) *Biochemistry 30*, 830−839.
42. Tamura, N., and Cheniae, G. M. (1986) *FEBS Lett. 200*, 231−236.
43. Miyao Tokutomi, M., and Inoue, Y. (1992) *Biochemistry 31*, 526−532.
44. Allakhverdiev, S. I., Karacan, M. S., Somer, G., Karacan, N., Khan, E. M., Rane, S. Y., Padhye, S., Klimov, V. V., and Renger, G. (1994) *Biochemistry 33*, 12210−12214.
45. Ananyev, G. M., and Dismukes, G. C. (1996) *Biochemistry 35*, 14608−17.
46. Dismukes, G. C. (1988) *Chem. Scripta 28A*, 99−104.
47. Babcock, G. T., Blankenship, R. E., and Sauer, K. (1976) *FEBS Lett. 61*, 286−289.
48. Hundelt, M., Hays, A. M., Debus, R. J., and Junge, W. (1998) *Biochemistry 37*, 14450−14456.
49. Meunier, P. C., Burnap, R. L., and Sherman, L. A. (1995) *Photosynth. Res. 45*, 31−40.
50. Meunier, P. C., Burnap, R. L., and Sherman, L. A. (1995) *Photosynth. Res. 47*, 61−76.
51. Engels, D. H., Lott, A., Schmid, G. H., and Pistorious, E. K. (1994) *Photosynth. Res. 42*, 227−244.
52. Vass, I., Cook, K. M., Deak, Z., Mayes, S. M., and Barber, J. (1992) *Biochim. Biophys. Acta 1102*, 195−201.
53. Johnson, G. N., Rutherford, A. W., and Krieger, A. (1995) *Biochim. Biophys. Acta 1229*, 202−207.
54. Rova, M., Mamedov, F., Magnuson, A., Fredriksson, P. O., and Styring, S. (1998) *Biochemistry 37*, 11039−11045.
55. Razeghifard, M. R., Wydrzynski, T., Pace, R. J., and Burnap, R. L. (1997) *Biochemistry 36*, 14474−14478.
56. Forbush, B., Kok, B., and McGloin, M. P. (1971) *Photochem. Photobiol. 14*, 307−321.

BI982331I